Plasmon Dispersion at a Superconductor-Dielectric Interface

by

Sabrina Sarah

Submitted in partial fulfilment of the requirements for the degree of Master of Applied Science

At

Dalhousie University

Halifax, Nova Scotia

August 2019

I dedicate this thesis to my dear grandpa Md. Shahabuddin for being my undying source of love and life.

Table of Contents

List of Tables

List of Figures

Abstract

Dispersion of the plasmon behaviour at an interface between a dielectric and a superconducting material is studied and numerically analyzed considering the electron gas is moving along the interface at a temperature of 44 K greater than T_c, which is the critical temperature. The high-temperature superconductor, YBCO (Yttrium Barium Copper Oxide), is used as the superconducting material and air as the dielectric material. A normalized dispersion equation is used to study the plasmonic behaviour at the interface. Considering the electron stream to behave as a compressible gas, new surface plasmon wave solutions of the dispersion equation have been obtained. The normalized form of the derived dispersion equation is employed to study the behaviour of the plasmon dispersion numerically using typical superconductor material parameters found recently in a study. The results indicate the SPPs travelling along the electron stream and the SPPs travelling against the electron stream interact and engage in an exchange of energy. The exchange of energy leads to amplification of the surface plasmon polaritons and increase in its propagation length. These results have the possibility of leading to novel applications of plasmonic effects.

List of Abbreviations and Symbols Used

a	Fitting parameter
BCS	Bardeen-Cooper Theory
c	Speed of light in vacuum
$\bar{J}$	current density
k	Wave vector
L	Propagation length
m_{eff}	Effective mass of carriers
n	Carrier density
N	Temperature-independent total density of free carriers
N	charge carrier density
N_n	Normal Electron Densities
N_s	Superconducting electron
SPP	Surface Plasmon Polariton
SPR	Surface Plasmon Resonance
T	Operating temperature
T_c	Critical Temperature
TE	Transverse Electric
TM	Transverse Magnetic
v_d	Electron drift velocity
w	Normalized Power Volume Density
YBCO	Yttrium Barium Copper Oxide
B	Normalized Propagation Constant
β	Longitudinal propagation constant
γ	Damping factor
γ_S	Transversal propagation constant of superconductor
γ_D	Transversal propagation constant of dielectric
γ_c	Scattering rate
Δ	Normalized drift velocity of electrons
ε_0	Permittivity of free space

ε_∞	High-Frequency Permittivity
ε_d	Dielectric permittivity of dielectric
ε_m	Dielectric permittivity of metal
Θ	Characteristic temperature of the boson field
λ	Wavelength
ξ	Fitting parameter
ρ	charge density
τ	Relaxation time
Ω	Normalized angular frequency
ω	Angular frequency
ω_n	Normal electron plasma resonant frequency
ω_p	Plasma Frequency in general
ω_s	Plasma frequency of superconductor

Acknowledgments

I would like to thank my supervisor Professor Michael Cada for giving me this wonderful opportunity to conduct my graduate studies with his research team. I'm also grateful for his thorough guidance and feedback, inspiration and patience, and financial support all through the dissertation work. I would also like to acknowledge the financial support from Dalhousie's Faculty of Graduate Studies during my graduate studies.

Chapter 1 Introduction

1.1 Introduction

The surface plasmon polaritons (SPPs) are the bound oscillations of the electrons and light propagating along an interface between a conductor and a dielectric material. They can also be defined as electromagnetic waves propagating along metal-dielectric interfaces.

Researchers have been studying the advantages of surface plasmon polaritons, which can be harnessed and implemented in various applications such as in near-field optics, subwavelength optics (waveguides), data storage, solar cells, chemical sensors and biosensors [1]. Their prospect as information carriers can bridge the gap between the photonic and electronic technologies through applications in highly integrated nanophotonic devices.

1.2 Thesis Theme and Objective

Possible amplification of signals through an interaction of an electromagnetic wave with an electron stream was reported in [2] and [3]. The charge carriers supporting waves tied to an interface were reported in [4]. The plasmonic effects in the charge carriers such as in an electron gas were studied due to its interaction with travelling waves in a semiconductor [5].

Researches have studied various interface systems to understand and acquire desirable plasmonic effects. In all the studies they considered the electron cloud of delocalized electrons on a conducting surface to be moving when an electrostatic field is applied. The conductor, in this case, can be a metal or semiconductor with desired doping concentrations.

Metals are lossy since they are governed by the Ohm's law up to a certain temperature. In search of better alternatives, semiconductors or better materials and materials with gain are proposed [4]-[10]. Semiconductors are lucrative for they can be tailored to have desired features. Their optical and electronic features make them preferable for plasmonic effects. Dr. Cada conducted research with a semiconductor-dielectric interface in Ref [11]. He studied the plasmonic effect for an interface structure consisting of an n-doped semiconductor with moving electrons and a dielectric. The drawback of that study was that the interface system incurred losses due to damping. Even energy exchange was not significant enough to compensate for all the losses.

One intuitive approach would be to consider a lossless plasmonic material i.e. a superconductor for the conductor-dielectric interface system. Superconductors have zero DC resistance below a critical temperature and are expected to show better plasmonic behaviour in supporting electromagnetic waves. In this thesis, a detailed study of such plasmonic effects is performed at such an interface between air and a superconductor with moving electrons.

The main goals of this body of research are to-

1. Study plasmonic effects at the interface between a high-temperature superconductor, YBCO, with moving electrons and a dielectric, which is air.

2. Analyze the dispersion relation at the interface due to the interaction of the electric field of surface plasmon polaritons and the drifting electrons.

3. Obtain normalized dispersion plots for the zero-electron drift and varying non-zero electron drifts.

4. Determine the energy exchange between the SPPs and the electron stream during their interaction using solutions from the dispersion plots.

5. Obtain normalized power volume density plots of the SPPs propagating along the electron stream and the ones propagating against the electron stream for varying electron drift velocity.

6. Obtain the propagation lengths of the SPPs propagating along the electron stream and the ones propagating against the electron stream using the solutions from the dispersion plots for varying electron drift velocity.

7. Determine if the interaction of the surface plasmon polaritons and the drifting electron stream leads to amplification of surface plasmon polaritons.

1.3 Thesis Contribution

I propose the plasmonic dispersion at an interface between a dielectric and a superconductor with moving electrons. In this thesis, my focus is on Yttrium Barium Copper Oxide, YBCO, as the Superconductor material. The plasmonic dispersion was numerically studied by normalizing the key parameters Using Wolfram Mathematica simulation software. The dispersion relation of our studied structure is normalized, and it is applicable for any conducting material and dielectric. The set of objectives were met in this study. My contributions are summarized below:

1. We obtained a 2-D normalized dispersion plot for YBCO/air interface, which illustrates the dispersion relation at the interface when the surface plasmon polaritons interact with

the drifting electron stream for the zero-electron drift and non-zero electron drift with no damping.

2. We obtained 3-D normalized dispersion plots for YBCO/air interface, which illustrate the dispersion relation and the behaviour of its solutions at the interface when the surface plasmon polaritons interact with the electron stream with increasing drift velocity of electrons.
3. We obtained the solutions from the dispersion plots for the SPPs travelling along the electron stream and the SPPs travelling against the electron stream and utilized it to analyze the energy exchange between the surface plasmon polaritons and the drifting electrons for varying electron drift velocity.
4. We obtained unique dispersive behaviour at the superconductor-dielectric interface.
5. We obtained the normalized power volume density plots of the SPPs travelling along the electron stream and for the SPPs travelling against the electron stream for increasing electron drift velocity.
6. We obtained the propagation lengths using the imaginary values of the solutions of the dispersion plots for the SPPs travelling along the electron stream and for the SPPs travelling against the electron stream for increasing electron drift velocity.
7. Finally, we conclude from our results that both of the SPPs travelling along and against the electron stream undergoes amplification as the electron drift velocity increases at the interface.

1.4 Thesis Organization

The thesis is organized as follows: Chapter 2 presents an overview of the fundamental theories of Surface Plasmon Polaritons (SPPs), including the physical and mathematical explanations of wave propagation and dispersion relation at the interface. The properties of SPPs and the derivations of their dispersion relation use Maxwell equations on a metal/dielectric or conductor/dielectric interface. At the end of Chapter 2, two brief SPPs excitation methods are reviewed. Chapter 3 talks about the general concepts of superconductivity and properties of superconductors. In Chapter 4, an interface between a dielectric and superconductor is proposed. I start by discussing plasmonic behaviour in superconductors, followed by material selection and parameters derivation for the analysis of the plasmonic dispersion at the interface. The dispersion effects are numerically studied and analyzed here, followed by simulations. In Chapter 5, the power volume density and the propagation length of the SPPs are introduced and calculated in the analysis by implementing Mathematica simulation software. After analyzing the data, I confirm that this interface between dielectric and superconductor YBCO holds a unique dispersion relationship, and longer propagation length. In Chapter 6, I conclude the thesis discussing the possible improvements and suggestions for future work.

Chapter 2 Theoretical Background

This chapter discusses the general concept of surface plasmon polaritons such as fundamentals and basic properties of SPP at the interface between a conductor and a dielectric medium. It mainly talks about the dispersion behaviour among the basic properties of SPP at the interface of a conductor and a dielectric medium. The chapter ends with a discussion of two SPP excitation techniques.

2.1 Surface Plasmon Polariton (SPP): The background theory

The plasmon is a collective oscillation of conducting electron gas responding to an electric field, in metal, and a special phenomenon of plasma oscillation mode is called surface plasmon (SP). Surface plasmon polariton (SPP) is a coupled electromagnetic wave to the collective oscillation of the free carriers at the interface between any two materials where the real part of the dielectric function changes signs across the interface, which has a dielectric with the dielectric constant ε_d and a conductor or semiconductor material, which has a dielectric constant ε_m.

2.2 Basic properties of SPP at a single metal-dielectric interface

For studying the basic properties of surface plasmon polariton, its behaviour at a single metal-dielectric interface is considered. We considered a plane interface between two different media, a metal with permittivity $\varepsilon_m\,(\varepsilon_1)$ and a dielectric with permittivity $\varepsilon_d(\varepsilon_2)$. The simple geometric structure is shown in Figure 2.1.

Figure 2.1 Schematic view of SPPs propagating along a single metal-dielectric interface

We start with Maxwell's equations; the wave equation can be written as:

$$\frac{\partial^2 \vec{E}(x)}{\partial x^2} + \left(k\varepsilon - \beta^2 \vec{E}\right) = 0 \tag{2.1}$$

$$\frac{\partial^2 \vec{H}(x)}{\partial x^2} + \left(k\varepsilon - \beta^2 \vec{H}\right) = 0 \tag{2.2}$$

Where E and H represent the electric field and magnetic field respectively, k represents the wave vector and β is the propagation constant of the waves, which is the component of the wave vector in the propagating direction.

We expand the two Maxwell source-free curl equations to obtain the following coupled equations for the time-dependent field:

$$\frac{\partial E_z}{\partial y} - \frac{\partial E_y}{\partial z} = j\omega\mu_0 H_x \tag{2.3}$$

$$\frac{\partial E_x}{\partial z} - \frac{\partial E_z}{\partial x} = j\omega\mu_0 H_y \tag{2.4}$$

$$\frac{\partial E_y}{\partial x} - \frac{\partial E_x}{\partial y} = j\omega\mu_0 H_z \tag{2.5}$$

$$\frac{\partial H_z}{\partial y} - \frac{\partial H_y}{\partial z} = -j\omega\varepsilon_0\varepsilon_r E_x \tag{2.6}$$

$$\frac{\partial H_x}{\partial z} - \frac{\partial H_z}{\partial x} = -j\omega\varepsilon_0\varepsilon_r E_y \tag{2.7}$$

$$\frac{\partial H_y}{\partial x} - \frac{\partial H_x}{\partial y} = -j\omega\varepsilon_0\varepsilon_r E_z \tag{2.8}$$

We consider a propagating wave, which has a solution confined to the interface exponentially decaying in the perpendicular z-direction on both sides of the interface given by:

$$H_y(z) = H_2 \exp(i\beta x - k_2 z), z > 0 \tag{2.9}$$

$$H_y(z) = H_1 \exp(i\beta x + k_1 z), z < 0 \tag{2.10}$$

Where $k_i^2 + k_0^2 \varepsilon_i = \beta^2$ (2.11)

($k_i = k_1, k_2$ and $\varepsilon_i = \varepsilon_m$ for z < 0, $\varepsilon_i = \varepsilon_d$ for $z > 0$)

We now deduce fields within a scale factor. We consider the **TM** (transverse magnetic) wave, which has a magnetic field parallel to the interface and no solution exists for **TE (**Transverse

Electric) waves [2,3]. We use Equations 2.9 and 2.10 and assume that the interface of metal and dielectric lies in the x-y plane at z=0, the surface waves can be shown as in Figure 2.2.

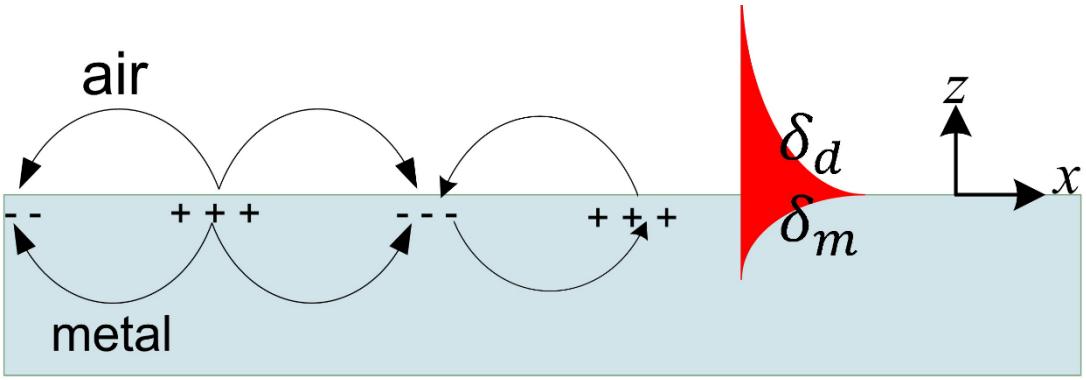

Figure 2.2: Schematic of the charges and the electromagnetic field of surface plasmon polariton propagating along a metal-dielectric interface in the x-direction together with the exponential dependence of the field, E, in the z-direction.

We apply the boundary conditions at the interface to obtain Equation 2.12:

$$k_m/k_d = -\varepsilon_m \,/\, \varepsilon_d \tag{2.12}$$

where ε_m and ε_d are the permittivity of the metal and dielectric respectively. From the above expression, we can infer the interface condition for the existence of the SPP. We find that the SPP exists and propagates at the interface between two different materials with opposite signs of dielectric permittivity.

We combine and simplify Equations 2.11 with Equations 2.12 and obtain the complex parallel wave vector in the x-direction and z-direction as:

$$k_x = k_x' + jk_x'' = \frac{\omega}{c}\left(\frac{\varepsilon_m \varepsilon_d}{\varepsilon_m + \varepsilon_d}\right)^{1/2} \tag{2.12}$$

where ω represents the angular frequency, c represents the speed of light in air vacuum, ε_d and ε_m are the relative permittivities of the dielectric and the conductor respectively. k'_x represents the real part which is associated with the surface plasmon wavelength and considered to be positive, whereas $k"_x$ causes damping decay. We replace $k'_x \; and \; k''_x$ to get the complex wavenumber as: $k_{spps} = k'_{spps} + jk''_{spps}$.

Considering $|\varepsilon''_m| \ll |\varepsilon'_m|$ and implementing the square root Taylor expansion to the first order, we can write Eq 2.14 as:

$$k_{spps} = k'_{spps} + jk"_{spps} = k_0 \sqrt{\frac{\varepsilon_m \, \varepsilon_d}{\varepsilon_m \, \varepsilon_d}} \frac{\left[1 + \frac{j\varepsilon"_m}{\varepsilon'_m}\right]}{\left[1 + \frac{j\varepsilon"_m}{2(\varepsilon'_m + \varepsilon_d)}\right]} \tag{2.13}$$

The real part which gives us the wave vector of SPPs is:

$$k'_{spps} = k_0 \sqrt{\frac{\varepsilon_m \, \varepsilon_d}{\varepsilon_m \, \varepsilon_d}} \tag{2.14}$$

and the imaginary part which is associated with the damping decay or loss:

$$k"_{spps} = \frac{k_0}{2} \frac{\varepsilon"_m}{\sqrt{\varepsilon'_m}} \left(\frac{\varepsilon_d}{\varepsilon_m + \varepsilon_d}\right)^{3/2} \tag{2.15}$$

Equation 2.14 shows the dispersion relation, whereas w=c is the light line. It is assumed that the near-medium is a perfect dielectric, ignoring the imaginary part for the moment. From Fig. 2.2, it can be seen that the evanescent damping decay of the fields is away from the interface. As shown, at the dielectric interface the amplitude is larger than at the metal interface; in fact, it is a few hundred nanometres at the dielectric interface and tens of nanometres at the metal interface.

In other words, when the imaginary part of the SPPs increases, the propagation length will decrease. Thus, the wavelength of SPPs can be written as:

$$\lambda_{spps} = \frac{2\pi}{k'_{spps}} = \frac{2\pi}{k_0}\sqrt{\frac{\varepsilon_m + \varepsilon_d}{\varepsilon_m\,\varepsilon_d}} \tag{2.16}$$

and the propagation length of SPPs as:

$$L_{spps} = \frac{1}{2k''_{spps}} \tag{2.17}$$

2.2.1 Dispersion Curves

Dispersion curve depicts the relationship between the propagation component of the wave vector and the wavelength. When we normalize the propagation component of the wavevector, we can refer the components as the propagation constant. This propagation constant is in turn considered as the effective refractive index of a waveguide and in this case, it is the interface.

The dispersion relation presented by the Drude dielectric function is given by:

$$\varepsilon_r = \varepsilon_\infty - \frac{{\omega_P}^2}{\omega(\omega + j\gamma)} \tag{2.18}$$

where ω_P represents the plasma frequency and γ is the damping factor of the metal, given by:

$$\omega_P = \sqrt{\frac{ne^2}{\varepsilon_0\, m^* m_0}} \tag{2.19}$$

where n is the carrier density, e is the electronic charge, $m^* m_0$ is the carrier effective mass, ε_0 is the permittivity of free space. We use a dielectric constant as well to account for losses. The Drude model in the z-direction will be in the form:

$$\varepsilon(\omega, z) = \varepsilon' + j\varepsilon'' = \varepsilon_\infty \left(1 - \frac{{\omega_P}^2}{(\omega^2 + \gamma^2)} + j\frac{{\omega_P}^2}{\omega(\omega^2 + \gamma^2)}\right) \tag{2.20}$$

where, ε_∞ is the high-frequency permittivity and γ is the damping term. When frequency almost reaches ω_P, damping becomes negligible. Drude dielectric function is then given by:

$$\varepsilon_r = \varepsilon_\infty - \frac{{\omega_P}^2}{\omega^2} \tag{2.21}$$

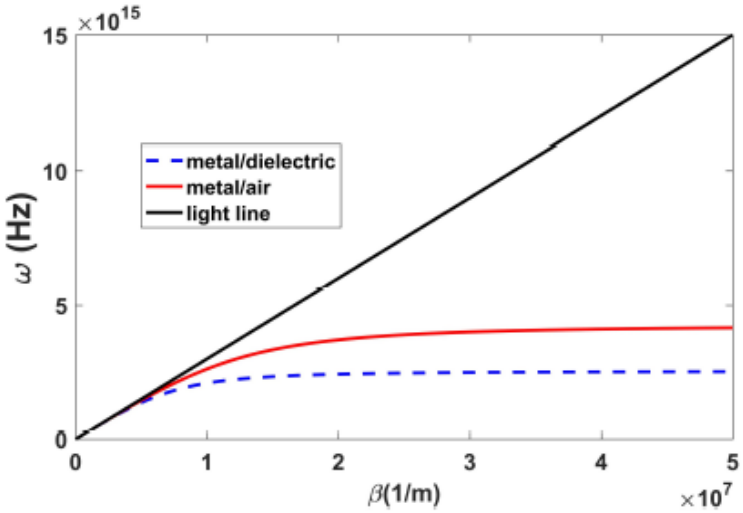

Figure 2.3: Dispersion relation of SPPs in metal/air (red curve) and in metal-dielectric (blue dash curve) interfaces. The black line indicates the light line.

Fig 2.3 shows that the SPP dispersion plots stay on the right side of the plot of the light in air. It implies that the wave vector of SPPs is always larger than that of the light in free space at given

frequencies. Hence, SPPs cannot form due to this mismatch of wave vectors. To excite SPPs, some techniques need to be implemented, which is discussed in the next section.

2.3 Excitation of SPPs at Planar Interfaces

The plots in Fig 2.3 present the SPP dispersion and line curves for two interfaces. If we observe the dispersion curve for the metal-air interface, we notice that it lies on the right side of the light line in the air. This implies that the wave number in the air is less than the propagation constant of the corresponding SPP mode at any given frequency. Hence the excitation of SPPs on a flat metal-air interface cannot be excited directly by light in the air due to the discrepancy or mismatch in the wavenumber, that's when the special phase matching techniques to excite SPP modes come into play. To achieve phase-matching the three-layer system can be introduced. The thin metal film is the middle layer sandwiched between the two dielectric layers with different dielectric constants. We can see a system with such a configuration in Fig 2.4. It is proposed by Kretschmann and is called the Kretschmann configuration.

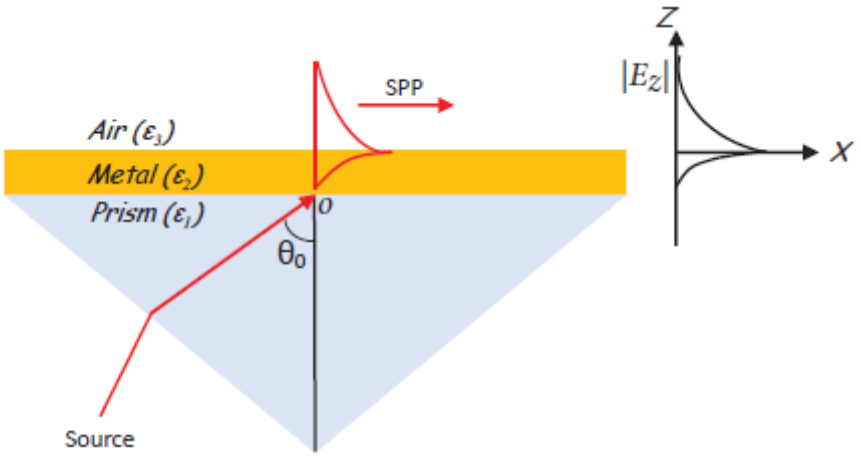

Figure 2.4: Prism coupling using the Kretschmann configuration

This Kretschmann configuration is used to excite SPPs at the metal-air interface. The incident light with wave vector magnitude k in the air will have a wave vector component $\beta = k_x = k\sqrt{\varepsilon_1 sin\theta_0}$ at the interface between the metal and the prism having propagated through the prism. Due to the higher refractive index of the prism in comparison to the air, the wave vector will now be significant enough to excite SPPs at the metal-air interface. Hence, SPP modes are excited with propagation constants β between the light line of air and that of the prism. In this configuration, the incident excitation field has to tunnel through the metal thin film to excite SPPs at the metal-air interface. There is also the Otto configuration, where a thin layer of air separates the metal and the prism as shown in Fig 2.5. This configuration is used for thick films where the Kretschmann configuration cannot be implemented and the contact with the metal surface is not necessary for its application. (In the Otto configuration, light undergoes total internal reflection at the prism-air boundary, so that the photons tunnel through the air gap between the surface and the prism.)

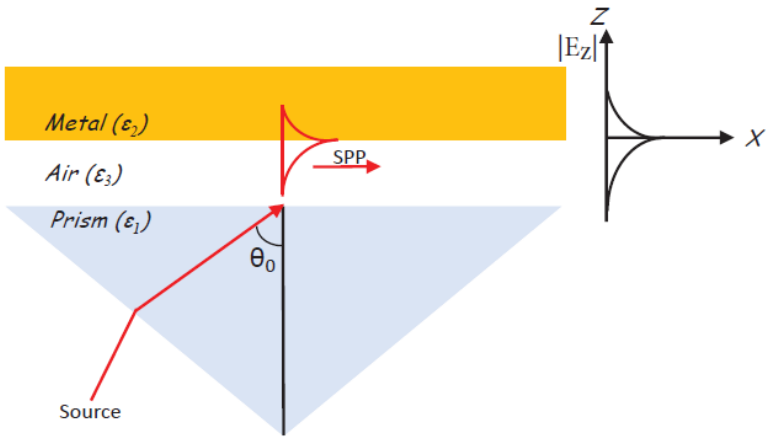

Figure 2.5: Prism coupling using the Otto configuration

There are other techniques of SPPs excitation but all the techniques increase the wavevector of incident light in the air in order to match the wavevector of SPP wave.

Chapter 3 Superconductivity

This chapter introduces the basic concepts of superconductivity. It also discusses the general behaviour of superconductors under the light of the BCS theory of superconductivity and how the electrons of the superconducting material behave below its critical temperature. It ends by outlining some of the experimental observations on superconductivity.

3.1 An Introduction to Superconductivity

Superconductors behave like any other material until its temperature drops down to a critical temperature Tc. Below the critical temperature, the material shifts to the superconducting state, which is determined by three unique properties: zero DC resistance, fully diamagnetic Meissner effect and macroscopic quantum coherence [12]. The superconducting state is characterized by three unique properties, not shared by normal metals: zero DC resistance, fully diamagnetic Meissner effect, and macroscopic quantum coherence. The macroscopic quantum coherence, in fact, results in the zero DC resistance and fully diamagnetic Meissner effect and results in effects such as the magnetic flux quantization and the Josephson effect [13].

3.2 Superconductivity: The BCS Theory

The BCS theory assumes that there must be an attraction force to overcome the Coulomb repulsion. This attraction can be a result of the coupling of electrons with the crystal lattice in case of low-temperature superconductors. When the free electrons move through the lattice, it attracts positive charges surrounding it. When the lattice deforms, another electron of opposite spin enters the

region of higher positive charge density. The two electrons correlate and appear as an electron pair, which couples for a range of three orders of magnitude larger than the lattice spacing, which can be hundreds of nanometers (over a range of hundreds of nanometers). This electron pair is famously known as Cooper pair. The formation of many Cooper pairs and their overlapping create a condensate. The Cooper pairs are qualitatively equivalent to the electron flow experiencing zero resistance. Thus, the condensate acts as a macroscopic coherent quantum state and is responsible for superconductivity. The total momentum of the Cooper pair is conserved in the direction of scattering [14].

The following expression is the conclusion of the BCS theory:

$$T_c \sim \Theta \, / \, e^{\frac{1}{\lambda}} \tag{3.1}$$

T_c is the transition temperature, below which a material shows superconductivity, Θ is the characteristic temperature of the boson field, and λ is the coupling constant of the boson field to electrons or holes. A large value of lambda makes metals good superconductors even if they are poor metals. Hence, metals like gold, silver, sodium and copper are good metals but not superconductor but lead is [15].

The Meissner effect, the dependence of the temperature of the energy needed to break the superconducting state and the Josephson effect are also supported by the BCS theory.

3.3 Some Experimental Facts on Superconductivity

The world of superconductors still holds a lot of unanswered questions and mysteries. The researchers are yet to account for all of its experimental observations. Some of the relevant experimental observations on superconductors are listed below:

- Superconductivity is limited by the critical temperatures of the superconductors. The superconductors will exhibit zero electrical resistivity as long as the temperature is below the critical temperature.
- Superconducting current can sustain without the presence of external interference or disturbance.
- Depending on the differences in reaction to magnetic flux, the superconducting material can be categorized into Type-I and Type-II superconductors. The Type-II superconductors are usually the intermetallic compounds and possess high critical temperatures.
- The type-II superconductors are not easily affected by a high magnetic field.
- The critical temperature of a superconductor may vary under high pressure.
- Superconductivity is a consequence of a low-temperature phenomenon. No phenomenon of superconductivity has been reported below 100^0K.
- Superconductivity of a material and its critical temperature is not correlated with its physical properties such as crystal structure, atomic number, ionization potential, etc.

Chapter 4 Plasmon Dispersion

The chapter begins with a discussion of the plasmon dispersion at a conductor-dielectric interface. It proceeds with the basic theory behind the plasmon dispersion at a conductor/dielectric interface and then laying out the equations that led to the final normalized dispersion equation, implemented in our study. Section 4.2 describes the mathematical model implemented in our study on plasmon dispersion at the superconductor/dielectric interface. Section 4.5 presents how the study on dispersion effects is performed implementing the normalized dispersion equation followed by the simulations.

4.1 Plasmon Dispersion at a Superconductor-Dielectric Interface: Basic theory

As mentioned in section 2.1, The excitation of surface plasmon polaritons along the interface of a conductor-dielectric interface causes the propagation of the surface electromagnetic plane wave along the interface. The dispersion relation of the surface plasmon polaritons is used in this study to depict the relationship between the longitudinal propagation constant of the wave and the angular frequency, which indicates their plasmonic behaviour at the interface.

In this study, we investigated the plasmonic effects at a superconductor-dielectric interface due to the interaction of the surface plasmon polaritons and the drifting electrons on the superconductor surface of the interface. The study is expected to reveal unique trends of the dispersive behaviour of the surface plasmon polaritons.

We proposed the geometry of a planar interface in which a superconductor with permittivity ε_s and a dielectric with permittivity ε_{d} are in contact. The superconductor surface

consists of a drifting electron gas due to an applied DC field. This drifting electron gas interacts with the electric field of the surface plasmon polaritons. The electron gas is considered to be compressible and thus its motion changes upon interaction with the surface plasmon polariton. The field of the surface plasmon polaritons modulates the electron stream supporting the surface plasmon polaritons along the structure due to applied DC drift. This current modulation is determined by the plasmonic properties of the drifting electron stream and the propagating polaritons.

The appropriate boundary conditions satisfy for longitudinal components of the fields of the interacting wave. These boundary conditions decide the outcomes of interaction, allowing an energy exchange between the drifting electrons and the propagating surface plasmon polaritons. The velocities of the slow propagating polaritons and that of the electron stream should be comparable leading to an energy exchange so that one can pick up the energy dissipated by the other.

The energy exchange, facilitated by the interaction between the propagating polaritons and the drifting electrons, creates a possibility of amplification of the plasmonic wave in the superconducting medium.

We studied the dispersion effects at our proposed interface by employing a normalized dispersion equation derived by Dr.Cada in [11]. The dispersion relation in [11] has been efficiently constructed and normalized to make it ideal for the analysis of any conductor-dielectric interface. This numerical analysis permits the observation of dispersion effects for our cases of interest, such as zero-electron, non-zero electron drift and increasing electron drift.

Section 4.2 discusses the superconductor material of our choice; its permittivity and parameters. Sections 4.3 elaborates the mathematical model of the dispersion relation.

4.2 Material Selection, Permittivity and Parameters

Our studied structure is an interface between air and a superconductor with moving electrons. The superconductor-dielectric interface has a high-temperature type-II superconductor with permittivity ε_s and a dielectric with permittivity ε_{d}. The superconductor considered for our case is YBCO (Yttrium Barium Copper Oxide) with a critical temperature of 88 K. YBCO loses its superconductivity above its critical temperature. The cost of the coolant makes YBCO a cheap option as well. Just like any other superconductor, it has zero DC resistance and acts as a lossless medium.

From the BCS theory and the two-fluid model explained in Ref. 21, the permittivity of YBCO under the critical temperature can be expressed by the Drude model:

$$\varepsilon_{2\_\mathrm{YBCO}} = \frac{\omega^2\tau^2(\omega^2 - \omega_{\mathrm{s}}^2 - \omega_{\mathrm{n}}^2) + (\omega^2 - \omega_{\mathrm{s}}^2)}{\omega^2(\omega^2\tau^2 + 1)} + i\frac{\omega_{\mathrm{n}}^2\tau}{\omega^3\tau^2 + \omega} \tag{4.1}$$

where τ is the relaxation time, ω, ω_{s} and ω_n represent the angular frequency, plasma frequency, and normal electron plasma resonant frequency respectively. τ, ω_{s} and ω_{n} are given by:

$$\tau = \frac{t^{\xi} + at\left(1 - t^{\xi}\right)}{t^{(1+\xi)\gamma_{\mathrm{c}}}}, \qquad \omega_{\mathrm{s}} = \sqrt{\frac{N_{\mathrm{s}}e^2}{m_0\varepsilon_0}}, \qquad \omega_{\mathrm{n}} = \sqrt{\frac{N_n e^2}{m_0\varepsilon_0}} \tag{4.2}$$

where a and ξ represent the fitting parameters, e is the unit electron charge, m_0 is the mass of a free electron, $t = T / T_c$, T_c and T stands for the critical and operating temperatures respectively, N represents the temperature-independent total density of free carriers, γ_c stands for the scattering rate at T_c , $N_s = N [1 - (T_c/T)^4]$ and $N_n = N(T_c/T)^4$ represent the superconducting electron and normal electron densities respectively. The parameters of Drude model for YBCO are [16]:

T_c = 88 K, ξ = 1.5, a=10, N = 1.255 × 10^{27} m^{-3}, γ_c = 0.28 × 10^{14} Hz. By substituting these values of parameter we obtain:

- $t = T / T_c$
- Relaxation time, $\tau = \frac{t^{\xi} + at(1-t^{\xi})}{t^{(1+\xi)}\gamma_c} = \infty$
- Superconducting Electron Density, $N_s = N [1 - (T_c/T)^4]$ = 1.177 × 10^{27} m^{-3}
- Normal Electron Density, $N_n = N(T_c/T)^4$ = 78.44 × 10^{24} m^{-3}
- Superconducting plasma frequency, $\omega_s = \sqrt{\frac{N_s e^2}{m_0 \varepsilon_0}}$ = 0.0374 × 10^{32} m^{-1}
- Normal electron plasma resonant frequency, $\omega_n = \sqrt{\frac{N_n e^2}{m_0 \varepsilon_0}}$ = 1.57 × 10^{11} m^{-1}

Generally, the background dispersive permittivity of conductors is also known as the high-frequency permittivity at high frequencies, which is evaluated by considering the ionic or lattice contributions. ε_∞ is the material high-frequency permittivity. A little simplification of the permittivity equation can provide the value of the high-frequency permittivity of YBCO as shown:

$$\varepsilon_{2_{\mathrm{YBCO}}} = \frac{\omega^2\tau^2(\omega^2 - \omega_\mathrm{s}^2 - \omega_\mathrm{n}^2) \times \frac{1}{\tau^2} + (\omega^2 - \omega_\mathrm{s}^2) \times \frac{1}{\tau^2}}{\omega^2(\omega^2\tau^2 + 1) \times \frac{1}{\tau^2}} + i\frac{\omega_\mathrm{n}^2\tau \times \frac{1}{\tau^2}}{(\omega^3\tau^2 + \omega) \times \frac{1}{\tau^2}}$$

$$= \frac{\omega^2 - \omega_\mathrm{s}^2 - \omega_\mathrm{n}^2}{\omega^2} = \frac{\omega^2 - \omega_\mathrm{s}^2}{\omega^2} = 1 - \left(\frac{\omega_\mathrm{s}}{\omega}\right)^2$$

Here $\omega_\mathrm{s}^2 >> \omega_\mathrm{n}^2$, therefore ω_n^2 can be neglected for simplification of the equation. The value of high-frequency permittivity of YBCO can be deduced as 1 ($\varepsilon_\infty = 1$). The permittivity of YBCO is negative here as $\omega < \omega_\mathrm{s}$ which means that the electric field vector and electric displacement vector point in opposite directions.

4.3 Dispersion Relation: The Mathematical Model

This section lays out the major mathematical equations that led to the formulation of the normalized dispersion equation that is implemented in the next section to study the dispersion effects at the proposed superconductor-dielectric interface. The complete derivation can be found in the Appendix of [11].

In section 4.1, we talked about electron compressibility, which gives the drifting electron stream its bunching nature during its interaction with the propagating wave along the structure. The field of the wave modulates the electron stream causing the electrons to speed up and down along the structure, supporting the surface plasmon polaritons along the structure due to applied DC drift.

The derivations shown below holds true for a two-dimensional case and for the propagation in the z-direction.

The basic defining equations are given below:

$$\nabla \text{x}\, \bar{H}_S = \bar{J} + \varepsilon_S \frac{\partial \bar{E}_S}{\partial t}\,;\;\; \nabla \cdot \bar{D}_D = 0\,;$$

$$m\frac{d\bar{v}}{dt} = -e(\bar{E} + \mu_0 \bar{v} * \bar{H})$$

$$\nabla \text{x}\, \bar{H}_D = \varepsilon_D \frac{\partial \bar{E}_D}{\partial t}\,;\quad \nabla \cdot \bar{H}_{S,D} = 0\,;\quad \varepsilon_{S,D} = \varepsilon_0 \varepsilon_{\infty,d}$$

$$\nabla \text{x}\, \bar{E}_{S,D} = \mu_0 \frac{\partial \bar{H}_{S,D}}{\partial t}\,;\quad \nabla \cdot \bar{J} = \frac{\partial \rho}{\partial t}\,;\quad \rho_0 = -eN$$

$$\nabla \cdot \bar{D}_S = \rho s\,;\; \bar{J} = \rho \bar{v}\,;\quad \omega_P = e\sqrt{\frac{N}{m\varepsilon_0}} \tag{4.3}$$

where $\bar{E}$, $\bar{H}$, $\bar{D}$ represent the electric, magnetic and displacement field vectors, respectively, $\bar{J}$, ρ, N represent the current density, the charge density, and the charge carrier density in the conducting medium (superconductor) respectively, $\boldsymbol{v}$ represents the velocity of the moving carriers (electrons), m=$m_0 m^*$ is the product of the free electron mass and its effective mass, $\boldsymbol{e}$ is the electron charge, ε_0 and μ_0 are the vacuum permittivity and permeability, respectively, ε_∞ and ε_d are the relative permittivity of the superconductor and the dielectric, respectively, ω_P is the plasma frequency, and subscripts *S* and *D* refer to the superconductor and dielectric materials, respectively. In our case, we assumed a superconductor, though the derivations are applicable to all conductors, provided material properties are relevant and used properly.

For a TM polarization in a two-dimensional case, when the x-axis is transversal and the boundary is along the z-axis, the current density, magnetic and electric field can be given by;

$$\begin{aligned} \bar{H}_{S,D} &= \{[0, H_{yS,D}, 0] \\ \bar{E}_{S,D} &= \left[E_{xS,D}, 0, E_{zS,D}\right] \\ \bar{J} &= [J_{xS}, 0, J_{zS}]\} \cdot \delta_{S,D} \end{aligned} \tag{4.4}$$

where $\delta_{S,D} = e^{-i\omega t} e^{-i\gamma_{S,D} x} e^{-i\beta z}$, w stands for the angular frequency, $\gamma_{S,D}$ and β represent the transversal and longitudinal; propagation constants, respectively.

For harmonic fields, the derivatives change to: $\frac{\partial}{\partial t} \longrightarrow -i\omega; \frac{\partial}{\partial x} \longrightarrow i\gamma_{S,D}; \frac{\partial}{\partial z} \longrightarrow i\beta.$

The velocity, the charge density and the current density are likely to have modulated constant amplitudes as shown:

$$\begin{aligned} \bar{v} = \bar{v}_0 + \bar{v}_S \delta_S &= [v_{x0} + v_{xS}\delta_S, 0, v_{z0} + v_{zS}\delta_S] \\ \rho = \rho_0 + \rho_S \delta_S \\ \bar{J} = \rho \bar{v} = \bar{J}_0 + \bar{J}_S \delta_S \end{aligned} \tag{4.5}$$

Substituting $\bar{J}_0 = \rho_0 \bar{v}_0$ in Eq (3.6) gives the following sets of equations

$$\begin{aligned} \bar{J} = \bar{J}_0 + \bar{J}_S \delta_S &= (\rho_0 + \rho_S \delta_S)(\bar{v}_0 + \bar{v}_S \delta_S) \\ \Rightarrow \bar{J}_S \delta_S &= \rho_S \bar{v}_0 \delta_S + \rho_0 \bar{v}_S \delta_S + \rho_S \bar{v}_S \delta_S \delta_S \end{aligned} \tag{4.6}$$

and:

$$\nabla \cdot (\bar{J}_0 + \bar{J}_S \delta_S) = -\frac{\partial(\rho_0 + \rho_S \delta_S)}{\partial t}$$
$$= \nabla \cdot (\bar{J}_S \delta_S) = -\frac{\partial(\rho_S \delta_S)}{\partial t} \tag{4.7}$$

When damping is taken into consideration, because of the free carrier collisions, $\gamma = \frac{1}{\tau}$, where τ is the relaxation time, the velocity equation can be written as:

$$\frac{dv_{x,z}}{\partial t} - \frac{v_{x,z}}{\tau} = \frac{dv_{x,z}}{\partial t} + v_{x,z}\frac{dv_{x,z}}{\partial_{x,z}} + v_{z,x}\frac{dv_{x,z}}{\partial_{z,x}}$$
$$= -\frac{e}{m}\left(E_{x,zS} \mp \mu_0 v_{z,x} H_{yS}\right) \tag{4.8}$$

The components of current density and charge density are now expressed as:

$$J_{xS} = \rho_S v_{x0} + \rho_0 v_{xS} + \rho_S v_{xS}\delta_S$$
$$J_{zS} = \rho_S v_{z0} + \rho_0 v_{zS} + \rho_S v_{zS}\delta_S \tag{4.9}$$

$$\nabla \cdot (\bar{J}_S \delta_S) = J_{xS}\frac{\partial(\delta_S)}{\partial x} + J_{zS}\frac{\partial(\delta_S)}{\partial z} \tag{4.10}$$

$$= i\gamma_S J_{xS}\delta_S + i\beta J_{zS}\delta_S = -\frac{\partial(\rho_S \delta_S)}{\partial t} = i\omega\rho_S\delta_S$$

The amplitudes of the current and the charge densities are linked by an important relationship as follows:

$$\rho_S = \frac{1}{\omega}(\gamma_S J_{xS} + \beta J_{zS}) \tag{4.11}$$

The complete derivations leading to the dispersion relation at an interface between a conductor and a dielectric, with a drifting compressible electron on the conductor's surface, can be found in the Appendix of [11].

The parameters are normalized as shown below, which led to the normalized dispersion equation. Hence the equation becomes applicable to any conducting material and dielectric.

$$\Omega = \frac{\omega}{\omega_p};\ \mathrm{B} = \frac{\beta_C}{\omega_p};\ \Gamma = \frac{\gamma}{\omega_p};\ \Delta = \frac{v_d}{c};\ \ \Gamma_{D,S} = \frac{\gamma_{D,S} c}{\omega_p} \tag{4.12}$$

where $\boldsymbol{c}$ represents the speed of light in air or vacuum. Substituting the expression $\Omega - \mathrm{B}\Delta + i\Gamma$ by H as in $\mathrm{H} = \Omega - \mathrm{B}\Delta + i\Gamma$, simplified the equations further. the transversal propagation components can be written as:

$$\frac{\gamma_D^2 c^2}{\omega_p^2} = \Gamma_D^2 = \varepsilon_d \Omega^2 - \mathrm{B}^2$$

$$\frac{\gamma_S^2 c^2}{\omega_p^2} = \Gamma_S^2 = -\frac{\left(\Omega - \dfrac{\mathrm{BH} - \Delta}{\varepsilon_\infty \Omega \mathrm{H} - 1}\mathrm{B}\right)\left[\mathrm{B}\Delta - \mathrm{H}(\Omega - \mathrm{B}\Delta)\left(\varepsilon_\infty \Omega - \dfrac{1}{\mathrm{H}\cdot}\right)\right]}{\mathrm{H}(\Omega - \mathrm{B}\Delta) - \dfrac{\mathrm{BH} - \Delta}{\varepsilon_\infty \Omega \mathrm{H} - 1}\Delta + \Delta^2} \tag{4.13}$$

The derivation of the dispersion equation can be found in [11]. Eqs. (4.12) and (4.13) are used to obtain the normalized dispersion equation of the interface:

$$\varepsilon_d^2\Omega^2(\Omega - B\Delta)^2 \times \left[H(\Omega - B\Delta) - \frac{BH - \Delta}{\varepsilon_\infty \Omega H - 1}\Delta + \Delta^2\right](\Omega - \frac{BH - \Delta}{\varepsilon_\infty \Omega H - 1} + (\varepsilon_d\Omega^2 - B^2) \times \left[\Omega - \frac{\varepsilon_\infty \Omega}{\varepsilon_\infty \Omega H - 1}(BH - \Delta)\Delta\right]^2 \times \left[B\Delta - H(\Omega - B\Delta)\left(\varepsilon_\infty \Omega - \frac{1}{H}\right)\right] = 0 \quad (4.14)$$

4.4 Implementation of Mathematical Model: Dispersion Relation at the Superconductor-Dielectric Interface

The normalized dispersion equation Eq. 4.14 derived in the previous section is employed in this section to study the dispersion effects at the superconductor-air interface. The mathematical model is implemented using Wolfram Mathematica software. Our study is divided into two sections. The first section talks about the simulations of the dispersion effects for zero electron and non-zero electron drift at the interface. The second section talks about the simulations of dispersion effects for increasing drift velocity of electrons at the interface.

The sections mostly include the following:

- obtaining the normalized dispersion plots and finding the solutions corresponding to SPPs of those dispersion plots
- analyzing the solutions to investigate what happens when the SPP is moving along the electron stream and when it is moving against the electron stream. The imaginary values of the solutions indicate gain since superconductors do not have attenuation.
- deducing from the table of solutions if the gain changes with the increase in electron drift speed.

The simulation results and solutions are given in the coming sections. The experimental parameters are given in Table 4.1.

TABLE 4.1**:** Experimental Parameters

Symbol	Quantity	Values
N	concentration [m^-3]	1.255×10^{27}
ε_{opt}	high-frequency permittivity	1
τ	relaxation time [fs]	∞
γ	damping factor	$\frac{1}{\infty} = 0$
ω_P	plasma frequency [rad/s] plasma wavelength [m]	1.933×10^{15} 0.975×10^{-6}
ω	operating frequency [rad/s] operating wavelength [m]	2.150×10^{14} 1.395×10^{-6}
T	operating temperature [K]	44

4.4.1 Implementation Using Mathematica

For this study, the normalized dispersion equation using a computational software known as Mathematica version 11.0. Mathematica is well known for its high precision computing. Mathematica is preferred for our study due to the following reasons:

- The Wolfram language is easier to learn as compared to other commercial software.
- It provides results with arbitrary precision.
- It can perform higher-order calculations by simply using single commands.
- It has elaborate documentation with live examples.
- It supports English language input and displays the proper syntax for the corresponding commands.
- Symbolic computation, complex numbers, interval arithmetic, contour plots, list plots are much simpler in Mathematica using only single commands, whereas other software requires forming multiple functions and loops.

4.4.2 Simulation of Dispersion Effects for the Zero and Non-Zero Electron Drift with Zero Damping

For this simulation, the relationship between the normalized longitudinal propagation constant, B, and normalized angular frequency, Ω, is analyzed for the zero-electron drift, $\Delta = 0$, and non-zero electron drift, $\Delta = 1/3 \times 10^{-3}$ and damping factor, $\gamma = 0$. B is given by $\mathrm{B} = \mathrm{B}' + i\,\mathrm{B}''$, where the real part B' decides how fast the wave travels and the imaginary part B" decides how much attenuation (absorption loss) or gain the wave undergoes. Since the damping factor γ is

zero, the longitudinal propagation constants are assumed to be real, i.e B = B', B" = 0. Thus a 2-D plot is used, which gives us a qualitative representation of the dispersion characteristic.

To perform the simulation of the dispersion effects for the zero and non-zero electron drift, the important steps are outlined below:

i. The normalized dispersion equation (Eq 4.14) and the normalization (Eq 4.12) are employed in this section for the simulation:

ii. The values of all the parameters except for B and Ω of Eq 4.14 are determined as given below:

- Relative permittivity of air, $\varepsilon_d = 1$
- High-frequency permittivity of YBCO, $\varepsilon_\infty = 1$
- Normalized electron drift velocity, $\Delta = 0, \frac{10^{-3}}{3}$
- Normalized damping factor, $\Gamma = 0$

iii. The values of parameters found in step (ii) are substituted into Eq 4.14. The normalized dispersion equation is then simplified to an implicit function of just two variables (B and Ω) such as f (B, Ω) = 0.

iv. The dispersion plot is then obtained by implementing the "Contourplot []" command in Mathematica software for $\Delta = 0$ and $3\Delta = 10^{-3}$ on the same axes. The 2-D normalized dispersion plot for YBCO/air interface is shown in Figure 4.1.

v. The value of the normalized angular frequency 'Ω' is determined for which the dispersion effect is prominent. This value of Ω is 0.699. The wavelength at which the dispersion effect is prominent is around 1.395 μm.

vi. The "Solve [] command was utilized in Mathematica software to obtain the numerical values of B for the plots when Ω = 0.699. The solutions of dispersion plots associated with SPPs for the cases of zero drift and non-zero drift without damping is shown in Table 4.2.

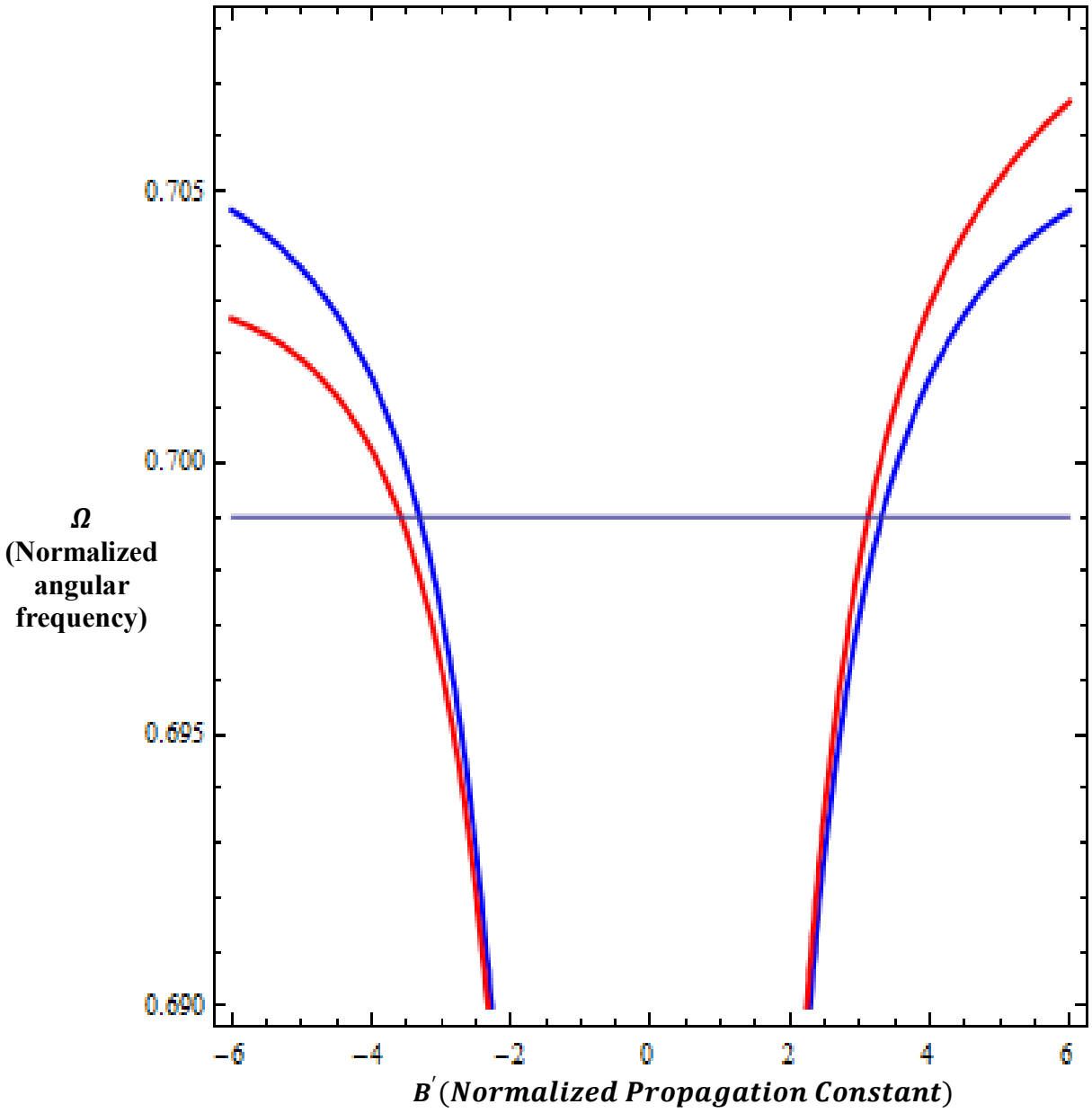

Figure 4.1: Normalized dispersion plots for YBCO-air interface; blue – zero electron drift, red – non-zero electron drift ($\Delta = \frac{1}{3} \times 10^{-3}$)

Table 4.2: Normalized Propagation Constants With Zero Damping (γ [s^ (-1)] =0)

Symbol	Quantity	Values	Values	Direction of motion
Δ	normalized electron velocity	0	1×10^{-3}	
B'	real part of propagation constants	+3.31062 -3.31062	+3.1180 -3.5838	along drift against drift
B"	imaginary part of propagation constants	0 0	0 0	along drift against drift

4.4.3 Simulation of Dispersion Effects for Increasing Electron Drift with Zero Damping

For the simulation of the dispersion effects for increasing electron drift, the normalized electron drift velocity 'Δ' is gradually increased and the corresponding solutions which are values of longitudinal propagation constant, B, associated to SPPs travelling along the electron stream and travelling against the electron stream are found following the steps of Section 4.4.2 as shown in Table 4.3.

The real and imaginary values of the propagation constants change with increasing electron drift velocity. The increase in electron drift affects the speed and attenuation or gain of the surface plasmon polaritons. Since YBCO is a superconductor, the imaginary values indicate gain. The change in SPPs' speed and gain caused by the increase in electron drift velocity is further studied in Ch-5 to investigate the energy exchange between the SPPs and the electron stream.

The 3-D plots are used to depict how the real and imaginary part of the propagation constants of the interacting surface plasmon polaritons vary with increasing electron drift velocity. These plots give a better illustration of the behaviour of the solutions associated with surface plasmon polaritons travelling along and against the electron stream. Figure 4.2 (a), (b) and (d) show the 3-D normalized dispersion plots where we observed how the dispersion effects vary as the electron drift velocity, Δ, increases from $1/3\times 10^{-5}$ to $1/3\times 10^{-3}$.

The solutions of the simulations of this section are utilized in the next section for investigating the energy exchange as a result of the interaction of the SPP and the drifting electrons.

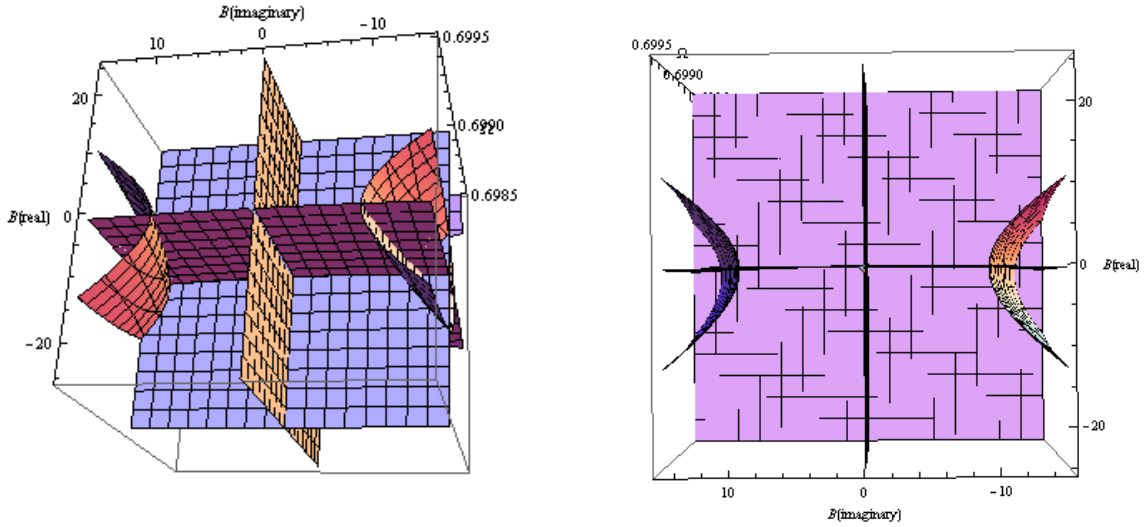

Figure 4.2 (a): Normalized 3-D dispersion plots for GaAs/air interface for $\Delta = \frac{1}{3} \times 10^{-5}$

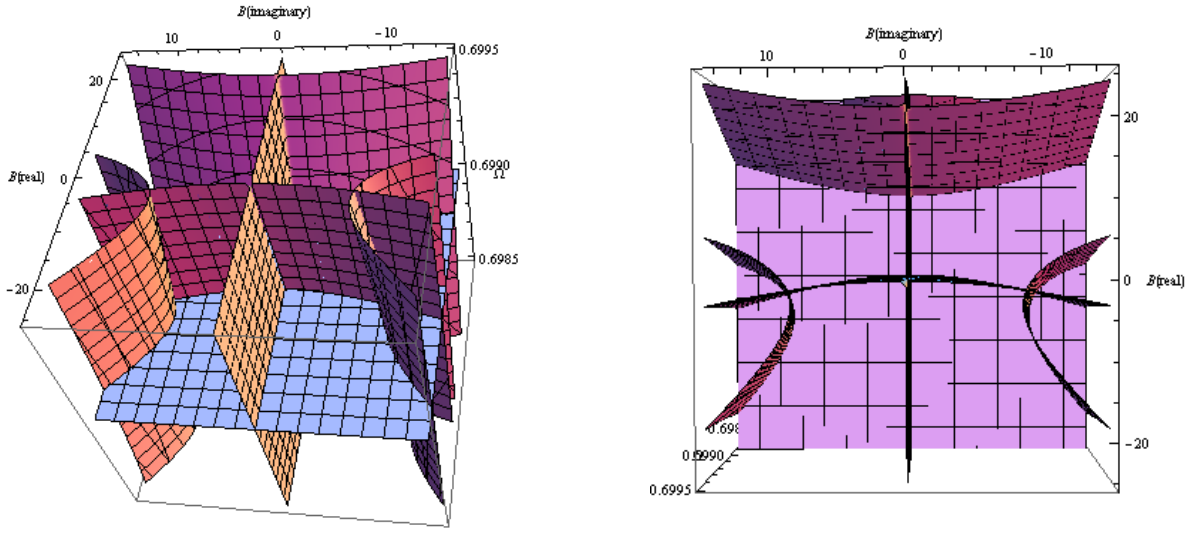

Figure 4.2 (b): Normalized 3-D dispersion plots for GaAs/air interface for $\Delta = \frac{1}{3} \times 10^{-4}$

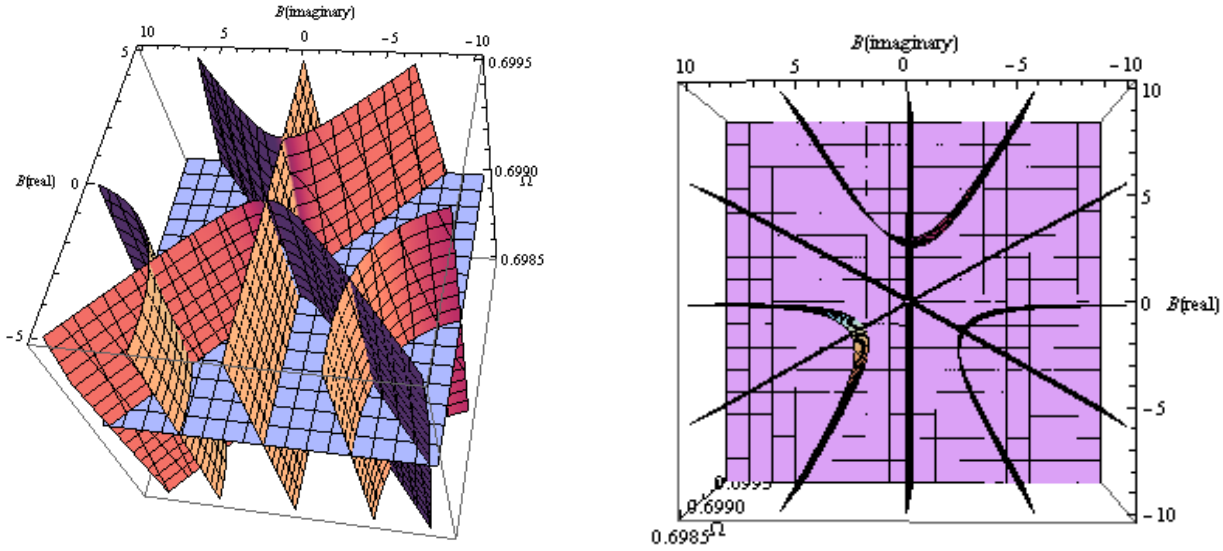

Figure 4.2 (c): Normalized 3-D dispersion plots for GaAs/air interface for $\Delta = \frac{1}{3} \times 10^{-3}$

Table 4.3: Normalized propagation constants with zero damping γ [s^ (-1)] =0 for the 3-D plot

Symbol	Quantity	Values	Values	Values	Direction of motion
Δ	normalized electron velocity	$1/3\times 10^{-5}$	$1/3\times 10^{-4}$	$1/3\times 10^{-3}$	
$B^{'}$	real part of propagation constants	-0.4659 -0.4648	-2.7117 -2.7113	-2.7088 -2.7080	along drift against drift
$B^{''}$	imaginary part of propagation constants	+12.6361 -12.6356	+10.7093 -10.7088	+5.5870 -5.5865	along drift against drift

Symbol	Quantity	Values	Values	Values	Values	Values	Direction of motion
Δ	normalized electron velocity	0.2×10^{-3}	0.4×10^{-3}	0.6×10^{-3}	0.8×10^{-3}	1.0×10^{-3}	
B'	real part of propagation constants	-2.9690 -2.9685	-2.6054 -2.6050	-2.3671 -2.3667	-2.1983 -2.1979	-2.0699 -2.0694	along drift against drift
B"	imaginary part of propagation constants	+6.5804 -6.5802	+5.2656 -5.2652	+4.6099 -4.6095	+4.1924 -4.1919	+3.8933 -3.8928	along drift against drift

Chapter 5 Energy Exchange

This chapter talks about the energy exchange that takes place due to the interaction of surface plasmon polaritons and the drifting electron stream at the superconductor-dielectric interface, followed by its consequence on the propagation length of surface plasmon polaritons. It starts by briefly explaining the energy exchange taking place between the surface plasmon polaritons and the electron stream, followed by the simulations of energy exchange and change in propagation length for the SPPs travelling along the electron stream and for those travelling against the electron stream.

5.1 Energy Exchange between SPP and Electron Stream

When the propagating wave and the drifting electron stream interact, the propagation constant of the wave changes as noticed in the simulation results of the previous section. The change in their imaginary values indicates an energy exchange during their interaction, provided the electron gas is assumed to be compressible. It can also be accounted for as the energy exchange between the surface plasmon polaritons and the applied electric field at the YBCO/air interface. The expression for the normalized time-averaged energy density also known as the power volume density is given in Eq 5.1.

$$\left\langle \frac{\partial w}{\partial t} \right\rangle = \frac{\omega_\rho}{c} P_{in} \times Re \left\{ i\mathrm{B} \left(\frac{\mathrm{BH} - \Delta}{\varepsilon_\infty \Omega \mathrm{H} - 1} \right)^* - i\Gamma_S \left[\Gamma_S \frac{\mathrm{H}(\Omega - \mathrm{B}\Delta) - \frac{\mathrm{BH} - \Delta}{\varepsilon_\infty \Omega \mathrm{H} - 1} \Delta + \Delta^2}{\mathrm{B}\Delta - (\Omega - \mathrm{B}\Delta)(\varepsilon_\infty \Omega \mathrm{H} - 1)} \right]^* \right\} \tag{5.1}$$

5.1.1 Simulation of Normalized Power Volume Density of SPP for Increasing Electron Drift.

For the simulation of this section, the solutions of the normalized dispersion plots were utilized to determine the time-averaged energy density of the surface plasmon polaritons. Important steps of the simulation are outlined below:

i. The values of normalized electron drift velocity, Δ, the corresponding values of $B^{'}$ and $B^{''}$ and the relevant experimental parameters were substituted into Eq. 5.1 to obtain the values of the time-average energy density 'w' (power volume density) of SPP.
ii. The drift velocity of the interacting electron stream is increased gradually and the corresponding value of the power volume density of the SPPs is determined. Table 5.1 lists the values of Δ, $B^{'}$, $B^{''}$ and w for SPPs travelling along the electron stream and for those travelling against the electron stream.
iii. The normalized power volume density plots were then obtained as a function of Δ, normalized electron drift velocity, for the surface plasmon polaritons travelling along the electron stream and for those travelling against the electron stream as shown in Figure 5.1 (a) and (b). The energy exchange plots depict how the energy exchange varies with increasing electron drift.

The power volume density 'w' of the surface plasmon polaritons travelling along and of those travelling against the electron stream increases as the normalized electron drift velocity increases gradually from 0.2×10^{-3} to 1.0×10^{-3}. Hence, the corresponding change in propagation length is investigated in the next section. The plots are obtained using the Wolfram Mathematica software.

Table 5.1: Normalized Power Volume Density of SPP with Zero Damping (γ [s^{-1}] = 0) for increasing electron drift velocity

Symbol	Quantity	Values	Values	Values	Direction of motion
Δ	normalized electron velocity	$1/3\times 10^{-5}$	$1/3\times 10^{-4}$	$1/3\times 10^{-3}$	
B'	real part of propagation constants	-0.4659 -0.4648	-2.7117 -2.7113	-2.7088 -2.7080	along drift against drift
B''	imaginary part of propagation constants	+12.6361 -12.6356	+10.7093 -10.7088	+5.5870 -5.5865	along drift against drift
$\left\langle\frac{\delta w}{\delta t}\right\rangle$	Time-averaged energy density (Power volume density)	+0.3315 × 10^6 -0.3300 × 10^6	+2.1391 × 10^6 -2.1382 × 10^6	+3.5084 × 10^6 -3.5077 × 10^6	along drift against drift

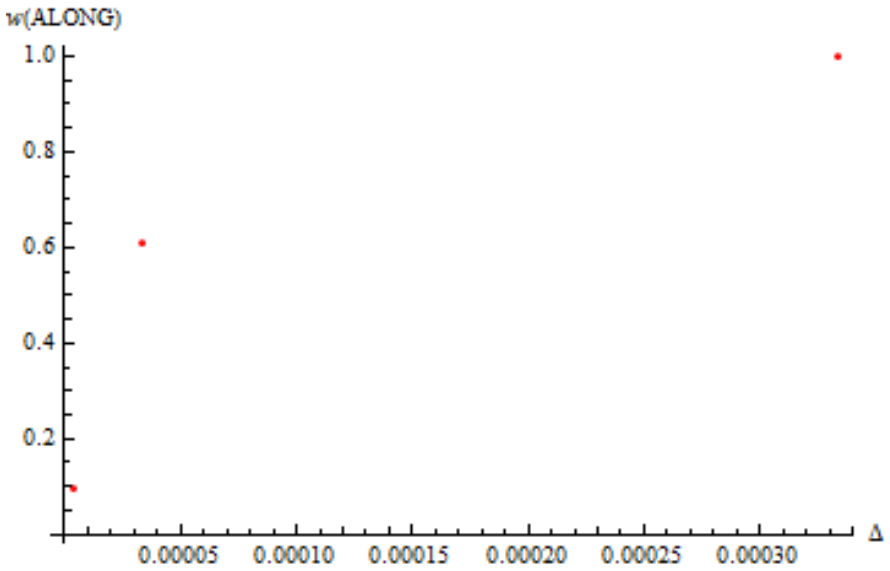

Figure 5.1: List Plot of Normalized power volume density of surface plasmon polaritons travelling along the electron stream

Figure 5.1 depicts only the normalized power volume density plot of SPP travelling along the electron stream as the normalized power volume density plot of SPP travelling against the electron stream is graphically identical to Figure 5.1. However, they differ numerically as shown in Table 5.1. As the electron drift velocity increases, the power volume density increases in both cases and the rate of increase is slightly higher when the SPPs are travelling along the electron stream.

5.2 Propagation Length of SPP for Increasing Electron Drift

The study of energy exchange in the previous section shows interesting results, which proposes a change in the propagation lengths of surface plasmon polaritons with increasing drift velocity. Hence, this section investigates the change in the propagation length of SPPs travelling along the electron stream and of those travelling against the electron stream.

5.2.1 Simulation of Propagation Length of SPP

For this simulation, the change in propagation length of the SPPs is determined using the imaginary values of the propagation constant B for corresponding normalized electron drift velocities as shown in Table 5.2.1. The plot of normalized propagation length as a function of normalized electron drift velocity shown in Figure 5.2 are produced in Wolfram Mathematica software.

Table 5.2: Normalized Propagation lengths of SPPs for YBCO/Air Interface as a function of normalized electrons velocity with zero damping γ [s^ (-1)] = 0

Symbol	Quantity	Values	Values	Values	Values	Values	Direction of motion
Δ	normalized electron velocity	0.2 $\times 10^{-3}$	0.4 $\times 10^{-3}$	0.6 $\times 10^{-3}$	0.8 $\times 10^{-3}$	1.0 $\times 10^{-3}$	
B''	imaginary part of propagation constants	+6.5804 -6.5802	+5.2656 -5.2652	+4.6099 -4.6095	+4.1924 -4.1919	+3.8933 -3.8928	along drift against drift
$L=\frac{1}{B''}$	Propagation Length of SPP	+0.15200 +0.15197	+0.18992 +0.18989	+0.21694 +0.21690	+0.23855 +0.23850	+0.25689 +0.25680	along drift against drift

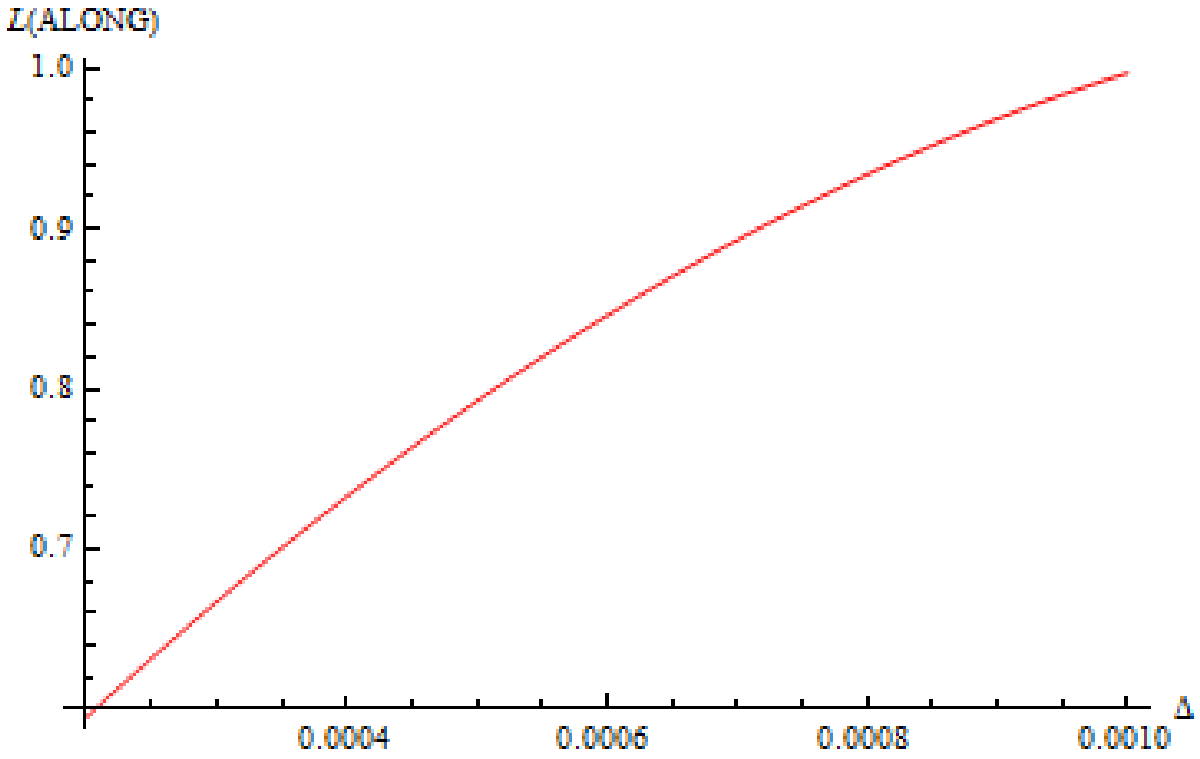

Figure 5.2: Normalized propagation length of surface plasmon polaritons travelling along the electron stream

The normalized propagation length plot of surface plasmon polaritons travelling along the electron stream is only presented in Figure 5.2. The normalized propagation length plot of SPP travelling against the electron stream is graphically identical to Figure 5.2, but it differs numerically as shown in Table 5.2. The power volume density and the propagation length values of the SPPs show a similar pattern. As the electron drift velocity increases, the propagation length increases when the SPPs are travelling along as well as against the electron stream, however the rate of increase is slightly higher when the SPPs are travelling along the electron stream.

5.3 Discussion

The power volume density plots for the SPPs travelling along the electron stream shows that the energy of the SPPs goes up as the electron drift velocity increases. It implies that the SPPs gain energy from the electron stream and undergoes amplification. The power volume density plots for the SPPs travelling against the electron stream shows that the energy of the SPPs also increases with increasing electron drift velocity which means the SPPs gain energy from the electron stream in this case as well and become amplified.

For both directions of interaction between the SPPs and the electron stream, the SPPs in the superconductor does not show attenuation but gain. The propagation length plots are also consistent with the power volume density plots, showing an increase in propagation length of SPPs travelling along the electron stream and of those travelling against the electron stream. The power volume density and propagation length of SPPs travelling the electron stream is slightly larger than those of SPPs travelling against the electron stream.

Chapter 6 Conclusion and Future Work

6.1 Conclusion

In this thesis, we study the dispersion characteristics of the superconductor-air interface system numerically for (i) zero electron drift, (ii) non-zero electron drift and (iii) increasing electron drift velocity with zero damping, as we choose a superconductor. For all the cases of study, the electrons in the superconductor surface are assumed to be a compressible gas of electrons moving along the interface. YBCO is chosen as the superconductor and air as the dielectric. YBCO is a high-temperature type-II superconductor.

The surface plasmon polaritons do not show any attenuation as there is no damping in a superconductor below its critical temperature. The electron drift velocity is increased to investigate whether the surface plasmon polaritons gets amplified upon interaction with the electron stream. The SPPs' propagation constant changes with increasing electron drift velocity. This implies that an energy exchange takes place between the surface plasmon polaritons and the drifting electron stream.

The SPPs travelling along the electron stream picks up energy from the electron stream and becomes amplified. The SPPs travelling against the electron stream also gains energy from electron stream with increasing electron drift. The propagation length increases with increasing drift velocity of electrons of the SPPs travelling along and also of those travelling against the electron stream. However, the power volume density and propagation length of SPPs travelling

along the electron stream is slightly higher than those of SPPs travelling against the electron stream.

The superconductor-dielectric interface has portrayed a unique dispersive trend of plasmon dispersion exhibiting gain and increase in propagation length in both directions of interaction (along and against) unlike other plasmonic materials such as metals and semiconductors. It can contribute to promising applications in the future such as amplifying or lossless plasmonic devices.

6.2 Future Work

All results are based on our assumptions and considerations. A future study can be held varying those assumptions and considerations such as the electron compressibility property.

Graphene can be an impressive alternative plasmonic material due to its zero-band gap and high carrier mobility. It is possible to simulate the normalized dispersion curve for graphene and perform the same analysis.

The study can be held for different superconductor materials and their results can be compared.

Future studies can hold analysis, design and optimization of the YBCO/air interface structure.

The study can be held to find better methods to the solutions of the normalized dispersion curve.

Bibliography

[1] Mao, Xiaoou, and Michael Cada. "Optical Surface Plasmon in Semiconductors." Integrated Photonics Research, Silicon and Nanophotonics. *Optical Society of America, 2013.*

[2] Raether, Heinz. "Surface plasmons on smooth surfaces." Surface plasmons on smooth and rough surfaces and gratings. *Springer, Berlin, Heidelberg,* 1988. 4-39.

[3] West, Paul R., et al. "Searching for better plasmonic materials. "*Laser & Photonics Reviews 4.6* (2010): 795-808.

[4] J. Zenneck. Propagation of plane em waves along a plane conducting surface. *Ann. Phys. (Leipzig),* 23(1):907, 1907.

[5] J. Homola, S. S. Yee, and G.Gauglitz, "Surface plasmon resonance sensors review," Sensor. Actuat. B-Chem. 54, 3-15 (1999).

[6] H. A. Atwater, "The promise of Plasmonics," *Sci. Am 296, 56-63.*

[7] Maier, Stefan Alexander. Plasmonics: fundamentals and applications. *Springer Science & Business Media, 2007.*

[8] Mei, Kenneth., and G-C. Liang. "Electromagnetics of superconductors." *IEEE transactions on microwave theory and techniques39.9 (1991)*: 1545-1552.

[9] A. D. Rakic, A. B. Djurisic, J. M. Elazar, and M.L. Majewski, "Optical properties of metallic films for vertical-cavity optoelectronic devices," *Appl. Opt. 37, 5271-5283 (1998).*

[10] A.J. Seeds, H. Shams, M. J. Fice, and C. C. Renaud, "TeraHertz photonics for wireless communications," *J. of Lightwave Technol. 33, 579-587 (2015).*

[11] Michael Cada and Jaromir Pistora. "Plasmonic Dispersion at an interface between a dielectric and a conducting medium with moving electrons." *IEEE Journal of Quantum Electronics, Vol 52, No.6, June 2016.*

[12] W.L. Barnes, "Surface plasmon-polariton length scales: a route to subwavelength optics," *Journal of Optics A: pure and applied optics, vol. 8, no. 4, p. S87, 2006.*

[13] J. Homola. *Surface Plasmon Resonance Based Sensors.* Springer Series on Chemical Sensors and Biosensors. Springer Berlin Heidelberg, 2006.

[14] Majedi, A. Hamed. "Theoretical investigations on THz and optical superconductive surface plasmon interface." *IEEE Transactions on Applied Superconductivity* 19.3 (2009): 907-910.

[15] Tsiatmas, Anagostis, et al. "Superconductor plasmonics and extraordinary transmission." *Applied Physics Letters* 97.11 (2010): 111106.

[16] Ma, Youqiao, et al. "Plasmonic properties of superconductor-insulator-superconductor waveguide." *Applied Physics Express* 9.7 (2016): 072201.